JACC: BASIC TO TRANSLATIONAL SCIENCE VOL. 10, NO. 1, 2025


ORIGINAL RESEARCH - CLINICAL

# Targeting the Gut-Heart Axis Improves Cardiac Remodeling in a Clinical Scale Model of Cardiometabolic Syndrome

Florence M. Herisson, PhD,[a,b] Gaston L. Cluzel, PhD,[a,b] Maria Antonia Llopis-Grimalt, PhD,[a,b] Aoife N. O'Donovan, PhD,[b,c] Fatma Koc, PhD,[b,c] Kavita Karnik, PhD,[d] Ieva Laurie, PhD,[d] Kirstie Canene-Adams, PhD,[d] R. Paul Ross, PhD,[b] Catherine Stanton, PhD,[b,c] Noel M. Caplice, MD, PhD[a,b]

## VISUAL ABSTRACT

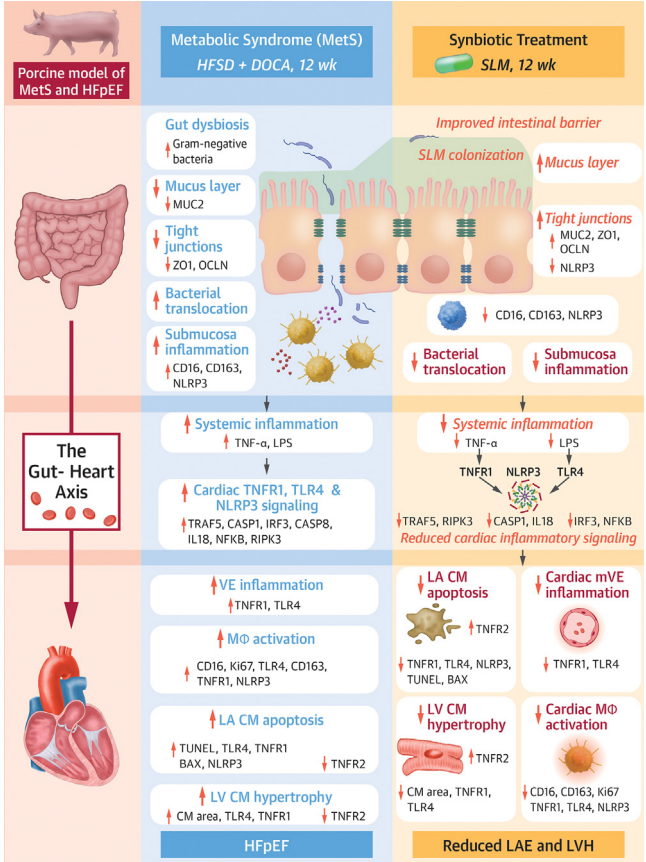


Herisson FM, et al. JACC Basic Transl Sci. 2025;10(1):1-15.

## HIGHLIGHTS

- In a porcine model of metabolic syndrome, HFpEF, and atrial myopathy, the full extent of the inflammatory GHA is demonstrated.
- The GHA extends from gut dysbiosis, barrier function loss, and bacterial translocation to systemic, microvascular, and parenchymal inflammation in the left heart chambers.
- Cardiac inflammation colocalizes with cardiomyocyte hypertrophy in the left ventricle and apoptosis in the left atrium.
- A synbiotic (prebiotic + probiotic) intervention targeted at the gut suppresses the GHA with reduced cardiac structural changes in the left heart of this model.

From the [a]Centre for Research in Vascular Biology, University College Cork, Cork, Ireland; [b]APC Microbiome Ireland, University College Cork, Cork, Ireland; [c]Teagasc Food Research Centre, Fermoy, Cork, Ireland; and [d]Tate & Lyle Solutions, LLC, Decatur, Illinois, USA.
The authors attest they are in compliance with human studies committees and animal welfare regulations of the authors' institutions and Food and Drug Administration guidelines, including patient consent where appropriate. For more information, visit the Author Center.

Manuscript received July 10, 2024; accepted September 9, 2024.

ISSN 2452-302X https://doi.org/10.1016/j.jacbts.2024.09.004

## ABBREVIATIONS AND ACRONYMS

**CM** = cardiomyocyte

**DOCA** = deoxycorticosterone acetate

**GHA** = gut-heart axis

**HFpEF** = heart failure with preserved ejection fraction

**HFSD** = high-fat, high-salt, high-sugar diet

**IL** = interleukin

**LA** = left atrium

**LM** = *Lactobacillus mucosae*

**LPS** = lipopolysaccharide

**LV** = left ventricular

**LVH** = left ventricular hypertrophy

**MetS** = metabolic syndrome

**Mφ** = macrophage

**mRNA** = messenger RNA

**mVE** = microvascular endothelium

**NFκB** = nuclear factor κB

**NLRP3** = nucleotide binding oligomerization leucine-rich repeat and pyrin domain 3

**SA** = sarcomeric actinin

**SLM** = synbiotic *Lactobacillus mucosae*

**TI** = terminal ileum

**TLR** = Toll-like receptor

**TNF** = tumor necrosis factor

**TNFR1** = tumor necrosis factor receptor 1

## SUMMARY

Poor diet, gut dysbiosis, and systemic inflammation constitute a gut-heart axis (GHA) that may affect heart failure with preserved ejection fraction. Clinical scale models to interrogate this axis are limited. Here, we show the full extent of the GHA–gut barrier function loss, systemic and microvascular inflammation, and its colocalization with apoptosis (left atrium) and hypertrophy (left ventricle). Gut barrier function primacy in regulating the GHA is supported by a synbiotic intervention that shuts down gut epithelial permeability, markedly decreasing systemic inflammation and, remarkably, cardiac structural changes in left heart chambers. These data support a new paradigm for targeting heart failure with preserved ejection fraction via the GHA.


Metabolic syndrome (MetS) represents one of the greatest health care challenges of the 21st century.[1] Left ventricular hypertrophy (LVH) and atrial myopathy, cardiac complications of MetS, contribute to heart failure with preserved ejection fraction (HFpEF),[2] a major cause of cardiovascular morbidity and mortality in the developed world. Therapeutic targeting of cardiometabolic disease is still nascent, with emerging success from use of sodium glucose cotransporter 2 inhibitors.[3] A key untargeted aspect of MetS remains low-grade systemic and organ-related inflammation, a recognized driver of cardiac structural changes in this disease, including LV cardiomyocyte (CM) hypertrophy, atrial fibrosis, and CM apoptosis.[4] This inflammation in part may originate from the gut, facilitated by impaired intestinal barrier function and reduced epithelial permeability, which itself is exacerbated by derangements in the gut microbiome.[5] Despite the likely importance of this gut-heart axis (GHA) in the transmission of inflammatory signaling from the gut mucosa to the cardiac parenchyma, little data are currently available on this interaction in clinical scale animal models.[6] Moreover, limited therapeutic intervention in the gut-heart inflammatory axis has occurred in cardiometabolic disease and HFpEF, with the major clinical focus being myocardial infarction and systolic HF.[7]

We previously characterized gut dysbiosis in a clinical scale porcine model of MetS/HFpEF that replicates many aspects of human disease. Specifically, we identified augmentation of proinflammatory and loss of anti-inflammatory bacterial populations during disease evolution.[8] However, data supporting a direct relationship between gut microbiota and structural changes within the heart during the development of MetS/HFpEF remain limited.[9] Moreover, little is known about the spatial and temporal links between inflammation in these organs that may facilitate targeting of regional inflammation in the gut with potential for the attenuation of cardiac-specific inflammatory sequelae, such as myocyte death and hypertrophy. In the current study, we examined the relationship between the temporal development of intestinal barrier function loss and increased gut permeability, transepithelial bacterial translocation and mucosal inflammatory cell mobilization, systemic inflammatory marker activation, and augmentation of resident inflammatory cells within the heart at the ventricular and atrial level in this MetS/HFpEF model. We posited that replacement of anti-inflammatory commensal bacterial populations might reverse inflammatory changes initiated at the gut barrier level. Moreover, we hypothesized that correction of the gut-heart inflammatory axis may have beneficial consequences for pathologic structural changes within the left atrium (LA) and LV seen in this disease.

## METHODS

We previously showed that a high-fat, high-salt, high-sugar diet (HFSD) and subcutaneous implantation of mineralocorticoid deoxycorticosterone acetate (DOCA) recapitulates most human aspects of gut dysbiosis, MetS, and cardiometabolic disease[8] in a domestic Landrace pig model. All gut microbiome, metabolic, biochemical, and hemodynamic indexes were fully characterized in our previous study.[8] In the current study, we used previous control (n =10) and MetS (n = 9) cohorts[8] to evaluate all inflammatory aspects of the GHA in these animals. In a separate group of experiments, an additional 24 animals were divided into 4 groups: MetS animals, as the control

group, were fed an HFSD + DOCA implant (n = 6), the second group (*Lactobacillus mucosae* [LM]) were fed similar diet + DOCA supplemented with $10^{10}$ colony-forming units/day LM DPC 6426 (n = 6), the third group (fiber) were fed HFSD + DOCA supplemented with 43 g/day PROMITOR 70 Soluble Fiber (Tate & Lyle LLC) (n = 6), and the fourth group (synbiotic *Lactobacillus mucosae* [SLM]) were fed with HFSD + DOCA supplemented with $10^{10}$ colony-forming units/day LM DPC 6426 and 43 g/day PROMITOR 70 Soluble Fiber (n = 6) (Supplemental Table 1, Supplemental Methods). Animals had free access to water at all times and were fed once per day and group housed. Pigs were fed with the respective diets over a 12-week period. All subsequent methods are described in the Supplemental Methods section.

**ETHICS.** All experimental procedures and application of the 3Rs[10] used during the study were reviewed and approved by the University College Cork Ethics Committee and Animal Welfare Body, under a license issued by the Health Products Regulatory Authority (reference numbers: AE19130-P041 and AE19130-P097) in exercise of the powers conferred on it under the European Union (protection of animals used for scientific purposes) Regulations 2012 (Systeme International no. 543 of 2012) as amended and Directive 2010/63/EU of the European Parliament and of the Council of 22 September 2010 on the protection of animals used for scientific purposes.

**STATISTICAL ANALYSIS.** Single animals were considered the experimental units, and all staining experiments compared controls vs MetS or MetS vs SLM. Data are presented as the median with 25th and 75th percentiles (Q1-Q3) or fold change of the mean with SD, unless otherwise specified. Comparisons between 2 groups used the Mann-Whitney *U* test, and comparisons among >2 groups used the Kruskal-Wallis test with the Dunn post hoc test for multiple pairwise comparisons.

To assess Gram-negative phylum-, family-, and genus-level changes in the pigs, significant taxa were analyzed by 2-way analysis of variance followed by the 2-stage step-up method of Benjamini, Krieger, and Yekutieli for multiple comparisons, with results presented as the mean ± SEM.

Untargeted level 1 and 2a metabolomic data underwent generalized logarithm transformation through MetaboAnalyst to permit parametric analysis. Data were found to have a normal distribution using plots and the Shapiro-Wilk test using the MetaboAnalyst metabolomics analysis suite.[11] To visualize clustering trends between MetS and control pigs, the unsupervised principal component analysis tool was performed on all metabolomic data.

Correlation of LV septal thickness measurement between echocardiography and postmortem tissue assessment was estimated by the Pearson correlation coefficient.

Analyses were conducted using GraphPad Prism version 8.1 for Windows (GraphPad Software, Inc), and a $P$ value of $<0.05$ was considered statistically significant.

**GHA IN A PORCINE MODEL OF CARDIOMETABOLIC SYNDROME.** In a previous study[8] by our group using control and MetS animals, we faithfully replicated the diastolic dysfunction porcine model first described by Schwarzl et al,[12] a model in which systolic function is normal (LV ejection fraction of >68%). We also previously confirmed by invasive hemodynamics that baseline LV end-diastolic pressure was significantly elevated (>50%; $P < 0.001$) in MetS animals compared to controls.[8] Moreover, LV end-diastolic pressure was increased (>85%; $P < 0.001$) after exposure to dobutamine stress in MetS animals vs controls,[8] consistent with an HFpEF phenotype described by Schwarzl et al.[12]

In the current study, we investigated the GHA (**Figure 1**) as it relates to small intestinal epithelial permeability and mucus barrier function loss; bacterial translocation; and intestinal, systemic, and cardiac inflammation within the LV and LA chambers in MetS animals vs control animals using our previous study cohorts.[8] Because macrophages (Mφs) were the most prominent inflammatory cells found within the gut submucosa and heart, we examined key inflammatory cytokines linked to regional activation of these cells.

## RESULTS

**MUCUS LAYER LOSS, INCREASED GUT PERMEABILITY AT THE EPITHELIAL LEVEL, AND AUGMENTED REGIONAL INFLAMMATION IN THE SUBMUCOSA OCCURS WITHIN THE TERMINAL ILEUM OF MetS ANIMALS.** MetS animals had significant loss of mucus layer within the terminal ileum (TI) after 12 weeks of HFSD compared to control animals (**Figure 1A**). This was accompanied by significant loss of antigenicity for MUC2 (Supplemental Figure 1A) as well as tight junction proteins ZO-1 (**Figure 1B**) and occludin (OCLN) (Supplemental Figure 1B). In the submucosa, there was increased $CD16^+$ (**Figure 1C**) and $CD11b^+$ (Supplemental Figure 1C) cells within the villi and crypts and increased $CD163^+$ cells (Supplemental Figure 1D) but no significant change in CD3

**FIGURE 1** **Intestinal Barrier Dysfunction, Mucosal Inflammation, Bacterial Translocation, and Systemic and Cardiac mVE Inflammation in MetS**

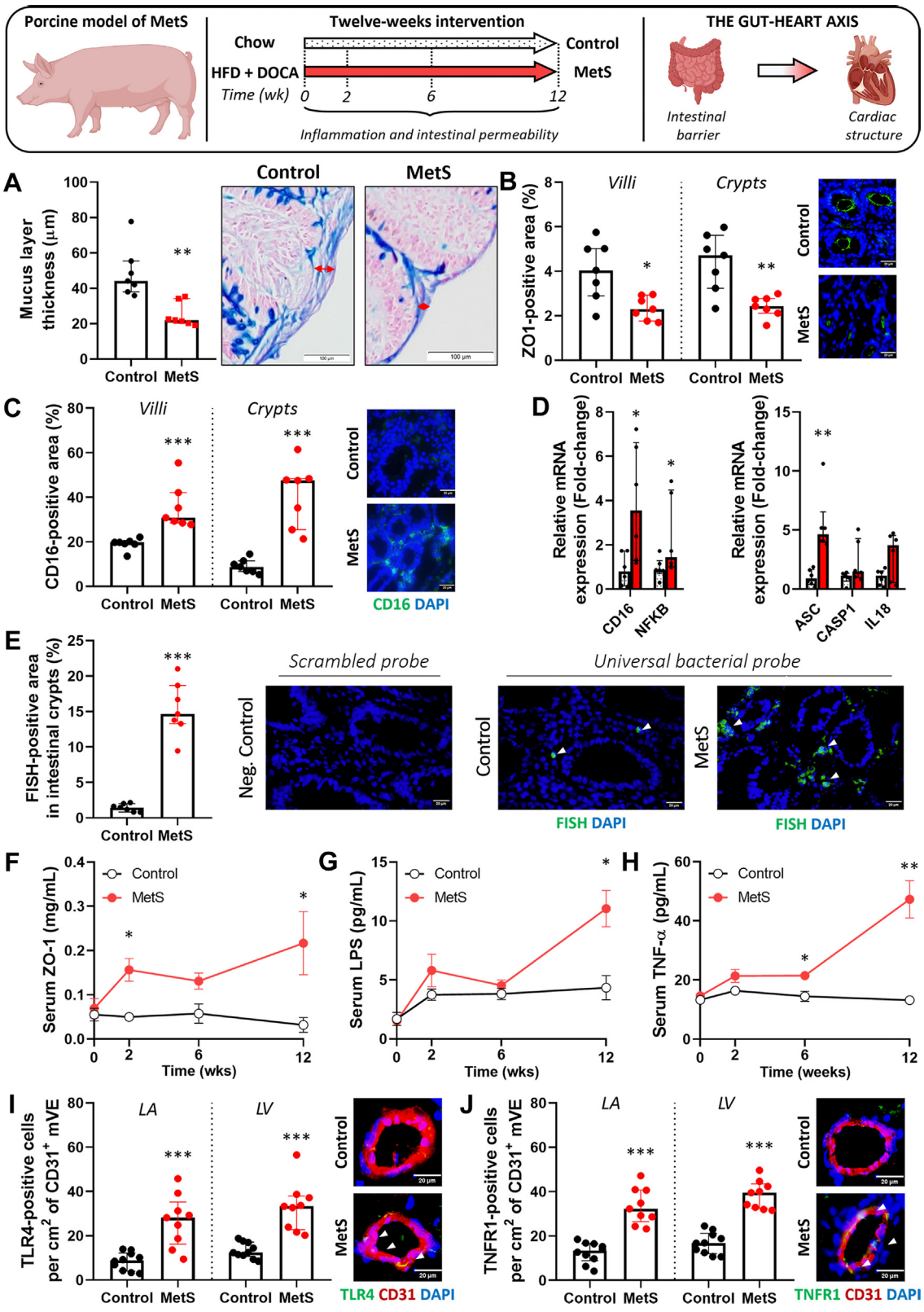


*Continued on the next page*

lymphocytes within the crypts (Supplemental Figure 1E). On CD16$^+$ cells, nucleotide binding oligomerization leucine-rich repeat and pyrin domain 3 (NLRP3) inflammasome expression was more than 3-fold higher in the MetS group compared to controls in both the villi and crypts (Supplemental Figure 1F). In the TI epithelium of MetS animals, NLRP3 expression was increased (Supplemental Figure 1G) and IGF1R expression was also increased, indicating activation (Supplemental Figure 2A). Increased *CD16* expression, nuclear factor κB (*NFκB*) activation and downstream signaling of NLRP3 (*Asc*, *Casp1*, and *IL 18*) were confirmed by messenger RNA (mRNA) analysis of TI submucosa in MetS animals compared to controls (**Figure 1D**). Proliferation of epithelial and CD16$^+$ cells by Ki67 index were similar in both treatment groups (Supplemental Figures 2B and 2C). Increased cell death via terminal deoxynucleotidyl transferase dUTP nick end (TUNEL) labeling was detected in the villi and crypts of MetS animals compared to controls (Supplemental Figure 2D), but this difference in TUNEL was not observed in CD16$^+$ cells (Supplemental Figure 2E).

**TIME COURSE OF INTESTINAL EPITHELIAL PERMEABILITY LOSS AND SYSTEMIC MARKERS OF BACTERIAL ENDOTOXEMIA AND Mφ ACTIVATION.** Fluorescence in situ hybridization signal for translocated bacteria in the crypt submucosa was approximately 30-fold higher in MetS vs control animals (**Figure 1E**). Moreover, MetS animals showed significantly increased ZO-1 release within the bloodstream as early as 2 weeks into the study when compared with control animals (**Figure 1F**). This increased circulating tight junction protein was maintained out to 12 weeks (**Figure 1F**). Similarly, endotoxemia marker lipopolysaccharide (LPS) (**Figure 1G**) and inflammatory cytokine tumor necrosis factor (TNF)-α (**Figure 1H**), known to be associated with Mφ activation, were elevated after 2 weeks and continued to rise to week 12 in MetS animals when compared to controls. Interestingly, Gram-negative bacterial populations in feces most commonly associated with LPS production were markedly increased at 2 weeks in MetS compared to control animals (Supplemental Figure 3).

At week 12, MetS animals also had significantly increased levels of markers of systemic inflammation (high-sensitivity C-reactive protein) (Supplemental Figure 2F), cytokines associated with pro- and anti-inflammatory Mφs (interferon gamma, IL-10), endothelial thrombogenicity (PAI-1), and NLRP3 inflammasome activation (IL-1β) (Supplemental Figure 2G). These systemic findings prompted analysis of specific cognate receptors in the microvascular endothelium (mVE) within the hearts of MetS and control animals. Immunostaining for Toll-like receptor (TLR) 4 and TNF receptor 1 (TNFR1) was markedly increased on mVE within the LA and LV of MetS animals compared to controls (**Figures 1I and 1J**).

**INFLAMMATION WITHIN THE LEFT HEART CHAMBERS OF MetS ANIMALS.** At the transcriptional level, there was significant increases in mRNA encoding *CD16*, *CD68*, *CD163*, *CD11b*, *CD206*, *CD3*, and *CD20* in the LA (**Figure 2A**) and LV (Supplemental Figure 4A). Using immunolabeling of cells to identify the specific location of inflammatory cells, there was a significant (>30%) increase in CD16$^+$ and CD163$^+$ cells within the LA of MetS animals compared to controls (**Figure 2B**). Subsequent colabeling studies using CD163 and CD16 showed costaining to approximately 90% between these antibodies, indicating that they identified similar Mφ-like cells in the heart and the spleen (Supplemental Figures 5A and 5B). Moreover, transcriptional analysis of *TIMD4* mRNA, known to be associated with resident Mφs, was significantly increased in the LA of MetS compared to control animals (Supplemental Figure 5C). In contrast, staining

**FIGURE 1 Continued**

Study of the gut-heart axis in control and MetS pigs fed, respectively, normal chow or HFD along with DOCA to induce hypertension over 12 weeks. (A) Intestinal mucus layer thickness (red arrows) by Alcian blue staining of TI sections. (B to D) TI immunofluorescence labeling of (B) ZO-1 and (C) CD16 in crypts and villi (control: n = 7; MetS: n = 7) and (D) relative mRNA expression of inflammatory and NLRP3 signaling genes (control: n = 6; MetS: n = 6). (E) FISH labeling of translocating bacteria within TI crypts (designated by arrowheads) with scrambled probe as negative control (control: n = 7; MetS: n = 7). (F to H) Temporal serum levels of (F) ZO-1, (G) LPS, and (H) TNF-α (control: n = 5; MetS: n = 5). (I, J) LA and LV immunofluorescence labeling of (I) TLR4 and (J) TNFR1 in the LA and LV within CD31$^+$ mVE area (designated by arrowheads) (control: n = 10; MetS: n = 9). All cropped or representative images were acquired at 600× magnification except for Alcian blue staining, which was imaged at 200×. Data are presented as median (Q1-Q3) and were compared using the Mann-Whitney test. *$P$ < 0.05, **$P$ < 0.01, and ***$P$ < 0.001. DAPI = 4′,6-diamidino-2-phenylindole; DOCA = deoxycorticosterone acetate; FISH = fluorescence in situ hybridization; HFD = high-fat diet; IL = interleukin; LA = left atrium; LV = left ventricle; MetS = metabolic syndrome; mRNA = messenger RNA; mVE = microvascular endothelium; Neg. = negative; NFKB = nuclear factor κB TI = terminal ileum; TLR4 = Toll-like receptor 4; TNF = tumor necrosis factor; TNFR1 = tumor necrosis factor receptor 1; TUNEL = terminal deoxynucleotidyl transferase dUTP nick end labeling; wk = weeks.

**FIGURE 2** LA Inflammation, NLRP3 Activation, CM Apoptosis, and Cytokine Receptor Signaling in MetS

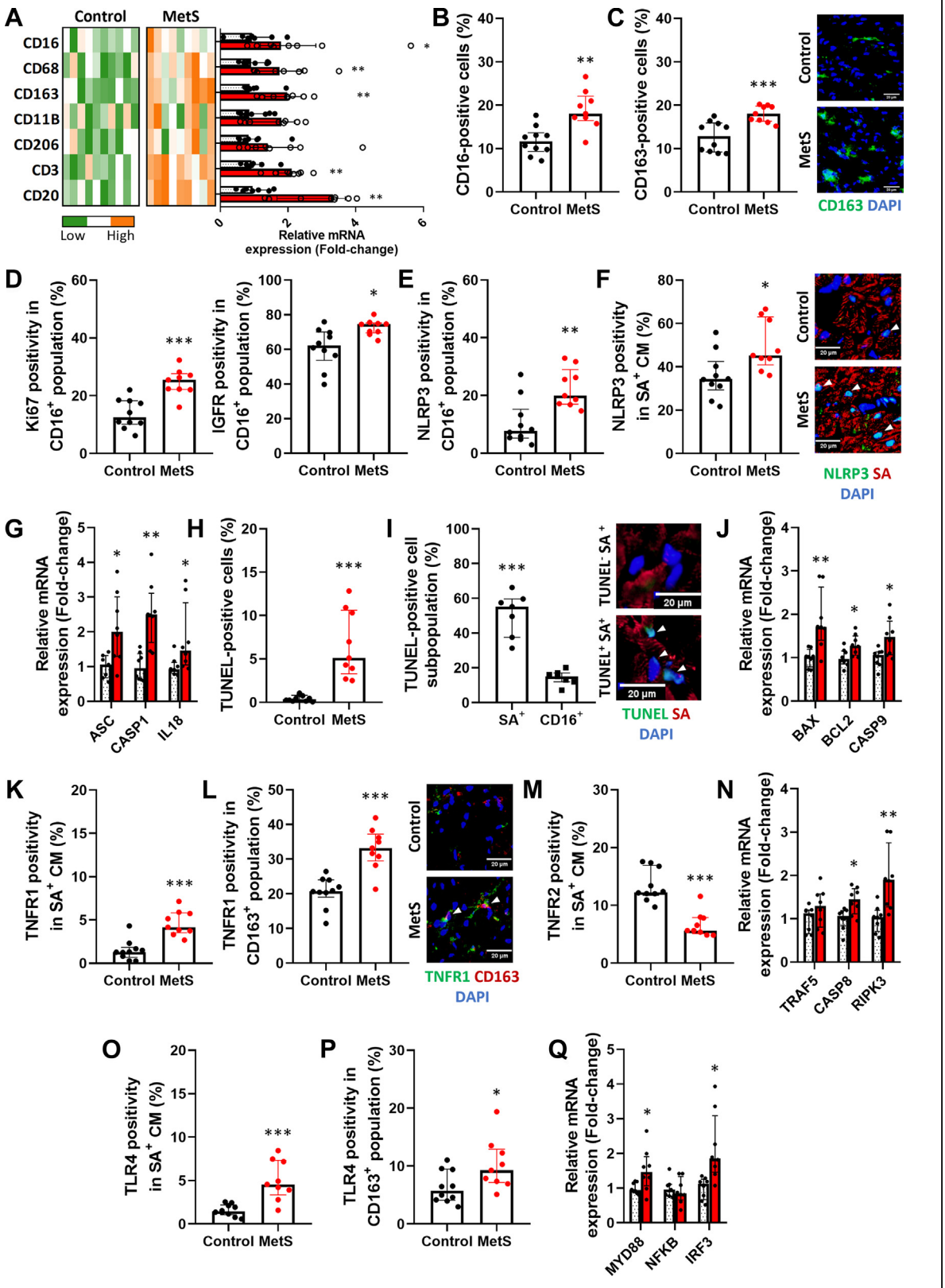


*Continued on the next page*

for fibroblasts showed no difference between animal groups (data not shown), nor did transcriptional analysis for markers of fibrosis including *COL1*, *COL3*, *ACTA2*, *PDGFA*, *FGF2*, or *TGFβ1* (Supplemental Figure 5D).

There was no increase in CD11B$^+$ cells in the heart of MetS animals (Supplemental Figure 4B), and CD68$^+$ and CD20$^+$ cells were undetectable in the hearts of all animals (data not shown). CD3$^+$ cells were 10-fold lower than CD16/CD163$^+$ cells, with a small but significant increase in these lymphocytes in the LA but not in the LV of MetS animals compared to controls (Supplemental Figure 4C).

**INCREASED NLRP3 INFLAMMASOME ACTIVATION, TNF AND TLR4 RECEPTOR EXPRESSION, AND CM APOPTOSIS IN THE LA OF MetS ANIMALS.** CD16$^+$ cells in the LA of MetS animals exhibited higher levels of Ki67 staining (**Figure 2D**) compared to control animals, indicating active proliferation as well as higher costaining with IGF1R (**Figure 2D**), a survival signal associated with activation of resident Mφs within tissues.[13] NLRP3 inflammasome was increased in CD16$^+$ cells (**Figure 2E**) as well as sarcomeric actinin (SA)$^+$ CMs within the LA of MetS animals (**Figure 2F**). Transcription associated with NLRP3 activation, including *ASC*, *Casp1*, and *IL18* mRNA, was also markedly increased in the LA of MetS animals (**Figure 2G**).

An inflammatory microenvironment is known to promote bystander cellular apoptosis,[14] and TUNEL staining showed a >20-fold increase in the LA of Mets animals with more than 80% of TUNEL signal colocalized with CMs (**Figures 2H and 2I**). Transcripts associated with apoptosis, such as *Bax*, *BCL2*, and *Casp9*, were significantly increased in the LA of MetS animals compared to controls (**Figure 2J**).

Given increased circulating TNFα and TNFR1 receptor staining in cardiac mVE of MetS animals, we assessed associated receptor expression of the proinflammatory TNFR1 and anti-inflammatory TNFR2 in the LA of these animals. TNFR1 staining was markedly increased in the LA of MetS animals and was colocalized with CMs (**Figure 2K**) and Mφs (**Figure 2L**), whereas TNFR2 staining, which colocalized only with CMs, was significantly reduced in the LA of MetS animals compared to controls (**Figure 2M**). RNA transcription indicative of TNFR1 signaling (*Casp8*, *RIPK3*) was increased in MetS animals compared to controls (**Figure 2N**). Similarly, TLR4 receptor expression within the LA was significantly increased in MetS animals compared to controls, and antigenicity was colocalized with CMs (**Figure 2O**) and Mφs (**Figure 2P**). Signaling transcripts downstream of TLR4, such as *MYD88* and *IRF3*, were both elevated in the LA of MetS animals (**Figure 2Q**).

**INCREASED Mφ INFILTRATION, INFLAMMASOME ACTIVATION, CYTOKINE RECEPTOR EXPRESSION, AND CM HYPERTROPHY IN THE LV OF MetS ANIMALS.** In the LV of MetS animals, a significant increase in CD16$^+$ cells (Supplemental Figure 4D) was detected with increased colocalization of Ki67 (Supplemental Figure 4D). Increased NLRP3 activation (*CD16*, *CASP1*) (Supplemental Figure 4E), as well as TLR4 immunoreactivity and signaling (SA, CD163, *NFKB*, *IRF3*) (Supplemental Figure 4F) were detected in MetS LV compared to controls. Similar to pathways observed in the LA, TNFR1 expression was increased and TNFR2 expression was decreased in the LV of MetS animals. In the LV, expression of TNFR1 was colocalized with Mφ immunoreactivity (Supplemental Figure 4G). Downstream signaling of TNFR1 was also increased in the form of *RIPK3* mRNA expression (Supplemental Figure 4G). These inflammatory indicators were present in association with increased CM hypertrophy in MetS compared to control animals and increased signal transcripts associated with hypertrophy (*MEF2D*, *RCAN1*, and *STAT3*)[15,16] (Supplemental Figure 4H).

**FIGURE 2 Continued**

(A) Relative mRNA expression of immune cell marker genes in the LA (control: n = 8 vs MetS: n = 8). (B to D) Immunofluorescence labeling of (B) CD16 and (C) CD163 as a percentage of total LA cells in control vs MetS and (D) Ki67 and IGFR labeling of CD16$^+$ Mφs (control: n =10; MetS: n = 9). (E) LA NLRP3 immunofluorescence labeling among CD16$^+$ Mφs, (F) SA$^+$ CMs (designated by arrowheads) (control: n = 10; MetS: n = 9), and (G) relative mRNA expression of NLRP3-associated genes (control: n = 8; MetS: n = 8). (H) TUNEL positivity in total LA cells in both groups (control: n = 10; MetS: n = 9) and (I) within CD16$^+$ and SA$^+$ cell populations (designated by arrowheads) in the MetS group (n = 7), and (J) relative expression of proapoptotic gene mRNA (control: n = 8; MetS: n = 8). (K to N) LA TNFR1 immunofluorescence positivity among (K) SA$^+$ CMs and (L) CD163$^+$ Mφs designated by arrowheads as well as (M) TNFR2 positivity among SA$^+$ CMs (control: n = 10; MetS: n = 9) and (N) relative mRNA expression of TNFR1-associated genes (control: n = 8; MetS: n = 8). LA TLR4 immunofluorescence positivity among (O) SA$^+$ CMs and (P) CD163$^+$ Mφs (control: n = 10; MetS: n = 9) as well as (Q) relative mRNA expression of TLR4-associated genes (control: n = 8; MetS: n = 8). All representative images were cropped from 600× magnification. Data are presented as median (Q1-Q3) and were compared using the Mann-Whitney test. *$P$ < 0.05, **$P$ < 0.01, and ***$P$ < 0.001. CM = cardiomyocyte; IGFR = insulin-like growth factor type 1 receptor; Mφ = macrophage; NLRP3 = nucleotide binding oligomerization leucine-rich repeat and pyrin domain 3; SA = sarcomeric actinin; other abbreviations as in **Figure 1**.

**SLM TARGETING OF THE GHA DECREASED PATHOLOGIC STRUCTURAL CHANGES IN THE LV AND LA OF MetS ANIMALS.** We previously showed that anti-inflammatory commensal bacteria were significantly reduced within 2 weeks of commencing HFSD in this porcine model,[8] with many bacteria almost completely absent by 12 weeks of study.[8] To counter this effect, we posited that feeding animals a well-characterized anti-inflammatory commensal LM may attenuate the gut effects of HFSD. Moreover, we hypothesized that the addition of a prebiotic fiber that LM can use as an energy source may increase residence of this bacteria in the intestine of treated animals. Synbiotics are combinations of probiotics and prebiotics that have positive effects on human health and are increasingly studied in microbiome research.[17] To determine the synergistic effects of a prebiotic fiber with a probiotic LM (SLM), we first examined cross-feeding effects of the fiber with LM and showed that the addition of fiber augmented bacterial growth in vitro (**Figure 3A**). We then tested the SLM intervention in vivo in the MetS model comparing 4 groups of animals fed HFSD alone, HFSD + fiber, HFSD + LM, or HFSD + SLM. Each group of animals was followed for 12 weeks, as in the previous MetS study (**Figure 3B**).

SLM intervention remarkably showed >20% reduction in LA dimension and LV wall thickness in MetS animals compared to MetS animals fed HFSD alone (**Figures 3C and 3D**). Moreover, neither the addition of LM alone or fiber alone had this effect on cardiac structure. Importantly, this change in LA size and LV thickness was hypertension independent because neither diastolic nor systolic blood pressure was significantly different among any of the 4 groups (**Figure 3E**, **Table 1**). To examine further whether SLM induced cardiac changes via the GHA, we compared robust readouts of barrier function (mucus layer), intestinal mucosal inflammation ($CD16^+$ cells), and low-grade systemic inflammation (blood TNFα) between all 4 groups. SLM significantly improved mucus layer production (**Figure 3F**) and reduced $CD16^+$ cells within the submucosa (**Figure 3G**) in the MetS group compared to the 3 other groups. Similarly, only SLM reduced levels of circulating TNFα in treated MetS animals to levels close to those observed in previous control animals without MetS (**Figure 3H**). No such changes were seen with LM or fiber alone treatments (**Figure 3H**).

We hypothesized that the positive cross-feeding effects of fiber observed in vitro (**Figure 3A**) might enhance in vivo LM survival within the gut of SLM-treated animals with positive therapeutic effects. To test this, we evaluated retained LM within the caeca of all 4 groups using polymerase chain reaction targeted at specific sequences within the LM genome. Cecal LM levels were markedly elevated in the SLM-treated group compared to the other 3 groups (**Figure 3I**).

**SLM REDUCED BACTERIAL TRANSLOCATION ACROSS THE EPITHELIAL BARRIER AND REDUCED EPITHELIAL PERMEABILITY AND SUBMUCOSAL INFLAMMASOME ACTIVATION IN CD16-POSITIVE CELLS IN MetS ANIMALS.** To investigate the mechanism by which SLM decreased structural changes in the LV and LA of MetS animals, extensive analysis of the previously characterized GHA was performed in SLM-treated and HFSD-only-treated MetS animals.

SLM significantly reduced bacterial translocation in the submucosa of treated animals compared to MetS only (**Figure 4A**). This was accompanied by significant increases in tight junction proteins, such as ZO-1 (**Figure 4B**) and OCLN (Supplemental Figure 6A) and, to a lesser extent, mucus-associated Muc-2 expression (Supplemental Figure 6B) on epithelial cells within the villi of SLM-treated vs control MetS animals.

SLM significantly reduced epithelial cell and submucosal $CD16^+$ cell-associated NLRP3 immunoreactivity compared to MetS animals (Supplemental Figures 6C and 6D). This was accompanied by significant down-regulation of mRNA transcripts associated with NLRP3 activation including *ASC*, *Casp1*, and *IL18* (Supplemental Figure 6E). Transcriptional activity associated with *CD16* cells and *NFκB* were also markedly reduced in the SLM-treated group compared to MetS animals (Supplemental Figure 6F).

**SLM REDUCED SYSTEMIC MARKERS OF ENDOTOXEMIA, GUT PERMEABILITY, AND INFLAMMATION WITH REDUCTION IN mVE EXPRESSION OF TLR4 AND TNF1 RECEPTORS IN THE HEART OF MetS ANIMALS.** To assess the temporal effects of SLM treatment, blood serum assays of bacterial endotoxemia (LPS), epithelial permeability (ZO-1), and systemic inflammation (TNF-α) were performed at 2 weeks, 6 weeks and 12 weeks posttherapy in MetS animals with or without intervention. From as early as week 2, posttreatment LPS was attenuated (at week 2 and week 12) by SLM therapy, and inhibitory effects of SLM on epithelial permeability (ZO-1 at week 12) and systemic inflammation (TNF-α, at week 6 and week 12) were evident throughout the study, with maximal effects seen at week 12 (**Figures 4C to 4E**).

At the end of the study, SLM also significantly reduced circulating levels of hs-CRP (**Figure 4F**),

**FIGURE 3** **Synbiotic Targeting of the Gut-Heart Axis Reduced Cardiac Structural Changes, Intestinal Barrier Dysfunction, Mucosal Mφ Abundance, and Systemic Inflammation in MetS**

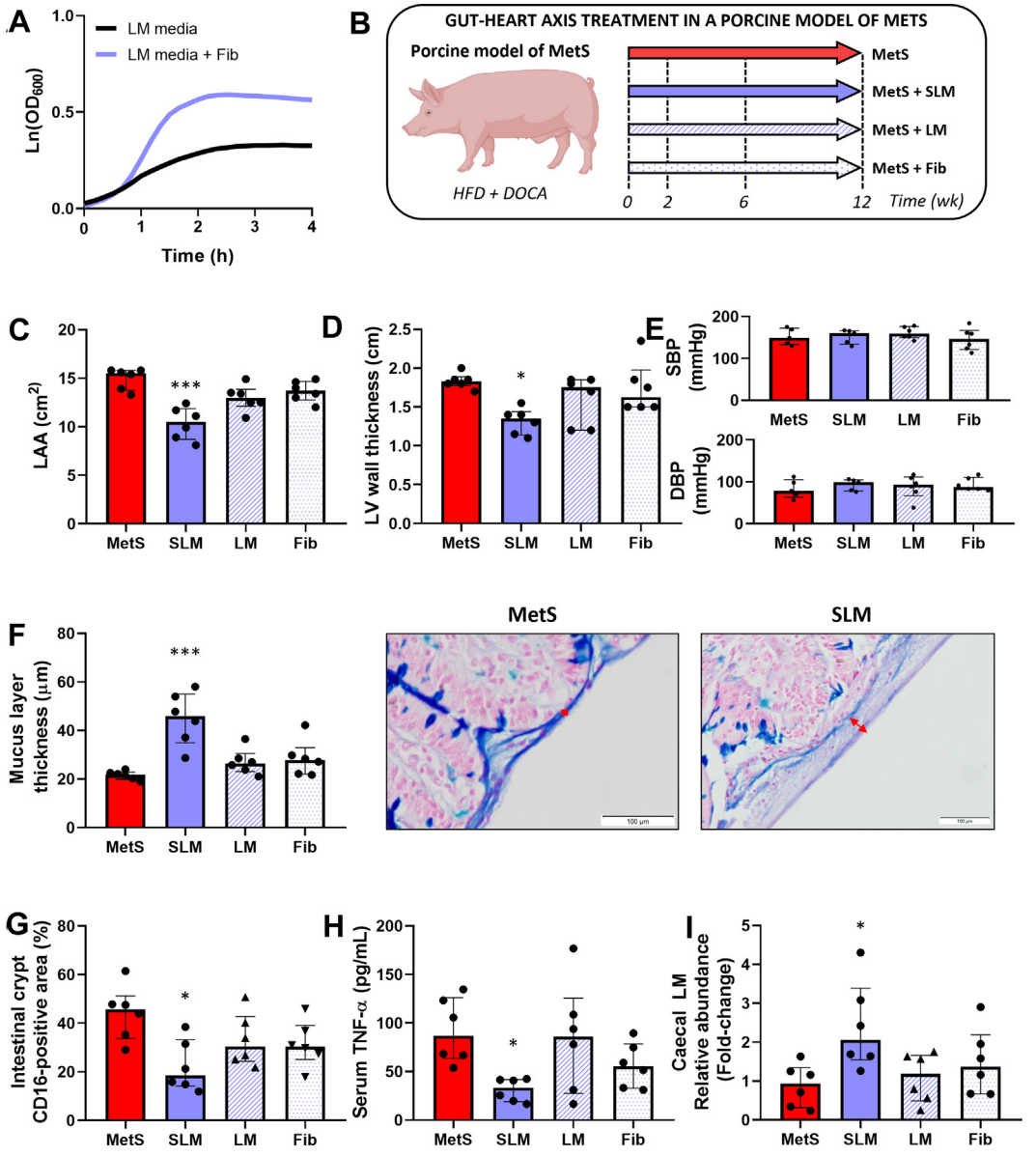


(A) LM growth curve in the presence or absence of fiber in media. (B) Gut-heart axis targeting of MetS using a synbiotic combination of LM and fiber (SLM) or individual LM or fiber. (C, D) Echocardiographic measurements of the (C) LAA and (D) LV wall thickness. (E) SBP and DBP at study termination. (F) TI mucus layer thickness measurements (red arrows) from Alcian blue staining images. Representative images were cropped from 200× magnification. (G) TI crypt immunofluorescence positivity of CD16. (H) Serum levels of TNF-α at the study end. (I) LM abundance measured by quantitative reverse-transcription polymerase chain reaction in cecal samples at study termination. MetS group (red): n = 6; SLM group (blue): n = 6; LM group (pale gray): n = 6; Fib group (speckled): n = 6. Data are presented as median (Q1-Q3) and were compared using the Kruskal-Wallis test. *$P < 0.05$ and ***$P < 0.001$. DBP = diastolic blood pressure; Fib = fiber; LAA = left atrial area; LM = *Lactobacillus mucosae*; OD = optical density; SBP = systolic blood pressure; SLM = synbiotic *Lactobacillus mucosae*; other abbreviations as in Figures 1 and 2.

interferon gamma, IL10 (Figure 4F), IL8 (Supplemental Figure 6), and PAI-1 (Figure 4F), as well as NLRP3 inflammasome marker (IL1β) (Figure 4F). With respect to cognate inflammatory cytokine receptors, SLM also markedly reduced cardiac mVE expression of TLR4 (Figure 4G) and TNFR1 (Figure 4H) within the LA and LV of treated animals when compared to control MetS animals.

**TABLE 1** MetS Parameters of Synbiotic-Treated Pigs

| | MetS | | | SLM | | | LM | | | Fib | | |
|---|---|---|---|---|---|---|---|---|---|---|---|---|
| | Median | Q1 | Q3 | Median | Q1 | Q3 | Median | Q1 | Q3 | Median | Q1 | Q3 |
| BW, kg | 70.8 | 66.5 | 76.7 | 67.2 | 58.8 | 71.4 | 66.7 | 65.2 | 69.5 | 71.0 | 64.9 | 72.8 |
| MBP, mm Hg | 119.5 | 101 | 138 | 131.8 | 107 | 140 | 123 | 116 | 143 | 117 | 97.3 | 139 |
| TAG, mg/dL | 33.7 | 24.7 | 35.4 | 18.25 | 14.9 | 24.7 | 20.53 | 8.25 | 42.8 | 22.49 | 8.78 | 42.8 |
| TC, mg/dL | 2,740 | 2,170 | 3,702 | 3,147 | 2,218 | 3,648 | 2,953 | 2,666 | 3,404 | 2,704 | 1,431 | 3,201 |
| HDL-C, mg/dL | 105.0 | 79.9 | 128.6 | 109.7 | 80.9 | 135.3 | 106.6 | 92.1 | 129.4 | 87.7 | 73.6 | 127.4 |
| LDL-C, mg/dL | 671.1 | 564 | 885 | 693.5 | 546 | 821 | 752.2 | 487 | 1,054 | 659.7 | 288 | 952 |
| LDL-C/HDL-C | 7.79 | 4.91 | 9.57 | 5.96 | 4.52 | 9.26 | 7.01 | 4.13 | 10.93 | 6.07 | 3.15 | 10.76 |
| FBG, mg/dL | 98.12 | 94.2 | 126 | 131.8 | 92 | 160 | 100.4 | 71.1 | 132 | 140.3 | 108 | 154 |
| FBI[a] | 1.44 | 0.76 | 1.88 | 0.87 | 0.43 | 1.26 | 0.64 | 0.43 | 1.71 | 0.74 | 0.51 | 1.27 |
| HOMA-IR[a] | 1.28 | 1.06 | 1.90 | 1.00 | 0.65 | 1.33 | 0.77 | 0.41 | 1.71 | 0.81 | 0.79 | 1.52 |

No significant difference between groups, estimated by a nonparametric Kruskal-Wallis test. Groups: MetS: n = 6; SLM: n = 6; LM: n = 6; Fib: n = 6. [a]FBI and HOMA-IR are expressed as fold change in comparison to baseline levels.

BW = body weight; FBG = fasting blood glucose; FBI = fasting blood insulin; Fib = fiber group; HDL-C = high-density lipoprotein cholesterol; HOMA-IR = homeostatic model assessment for insulin resistance; LDL-C = low-density lipoprotein cholesterol; LM = *Lactobacillus mucosae* group; MPB = mean blood pressure; SLM = synbiotic *Lactobacillus mucosae* group; TAG = triacylglycerol; TC = total cholesterol.

**SLM REDUCED Mφ ACCUMULATION IN THE LA, MARKEDLY REDUCING CM APOPTOSIS AND ATTENUATING NLRP3, TNFR1, AND TLR4 EXPRESSION.** $CD16^+$, $CD163^+$, and $CD11B^+$ cells within the LA were significantly reduced by SLM treatment compared to MetS-alone animals, whereas $CD3^+$ remained unchanged (**Figure 5A to 5D**). Moreover, *TIMD4* mRNA associated with cardiac resident Mφs was significantly reduced by SLM treatment compared to MetS alone (Supplemental Figure 6). With respect to the most prominent $CD16^+$ Mφs, the reduction in these cells caused by SLM treatment was associated with diminished cell proliferation (Ki67) (**Figure 5E**), with significant reduction in NLRP3 inflammasome activity in these cells (**Figure 5F**). Similar reduction in the NLRP3 inflammasome was detected in $SA^+$ CMs (**Figure 5G**). Moreover, mRNA transcription associated with NLRP3 activation, such as *casp1* and *IL18*, were both significantly attenuated by SLM treatment (**Figure 5H**).

We previously detected high levels of CM apoptosis in association with $CD16^+$ cell accumulation in the LA of MetS animals. Following SLM treatment, apoptosis within the LA of MetS animals was significantly reduced by >60% (**Figure 5I**), with reduction in apoptosis-associated RNA transcription (*Bax*) (**Figure 5J**), and this cell death reduction was detected in CMs but not in $CD16^+$ cells (**Figure 5K**). Two pathways implicated with Mφs in the heart and bystander CM apoptosis include TNF and TLR4 receptors.[18,19] SLM treatment reduced TNFR1 immunoreactivity in CMs (SA) (**Figure 5L**) and cardiac Mφs (CD163) (**Figure 5M**). Cytoprotective TNFR2 was increased on LA CMs of SLM-treated animals compared to MetS controls (**Figure 5N**), with reduction of mRNA transcripts associated with signaling downstream of TNFR1 activation (*Traf5* and *Ripk3*) (**Figure 5O**). SLM caused similar reductions in TLR4 immunoreactivity associated with CM (SA) (**Figure 5P**) and cardiac Mφs (CD163) (**Figure 5Q**), and reduced TLR4 downstream signaling was confirmed by reduced *IRF3* mRNA transcription in this treatment group compared to MetS controls (**Figure 5R**).

**SLM REDUCED Mφ ACCUMULATION AND PROLIFERATION AND NLRP3 EXPRESSION IN THE LV, SIGNIFICANTLY REDUCING CM SIZE (HYPERTROPHY), ATTENUATING TLR4 AND TNFR1, AND INCREASING TNFR2 EXPRESSION ON CMs.** SLM treatment reduced $CD16^+$, $CD163^+$, and $CD11B^+$ cells within the LV of treated animals vs controls (Supplemental Figure 7A to 7C). In $CD16^+$ Mφs, this was associated with a reduced proliferation index (Ki67) (Supplemental Figure 7D) and reduced coexpression of the NLRP3 inflammasome (Supplemental Figure 7E). CM hypertrophy was also reduced by approximately 30% in SLM-treated animals vs MetS controls (Supplemental Figure 7F). Consistent with previous data from the LA, SLM treatment also reduced TLR4 (Supplemental Figure 7G) and TNFR1 (Supplemental Figure 7H) expression in LV CMs but increased expression of the cytoprotective TNFR2 on these cells (Supplemental Figure 7I).

## DISCUSSION

Although there are emerging data on the role of the GHA in human cardiometabolic disease, the clinically relevant mechanistic foundations for this are limited by reduced access to human intestine and heart

**FIGURE 4** **Synbiotic Targeting of the Gut-Heart Axis Reduced Bacterial Translocation, Improved Tight Junction Protein Expression, and Reduced Systemic and Cardiac mVE Inflammation in MetS**

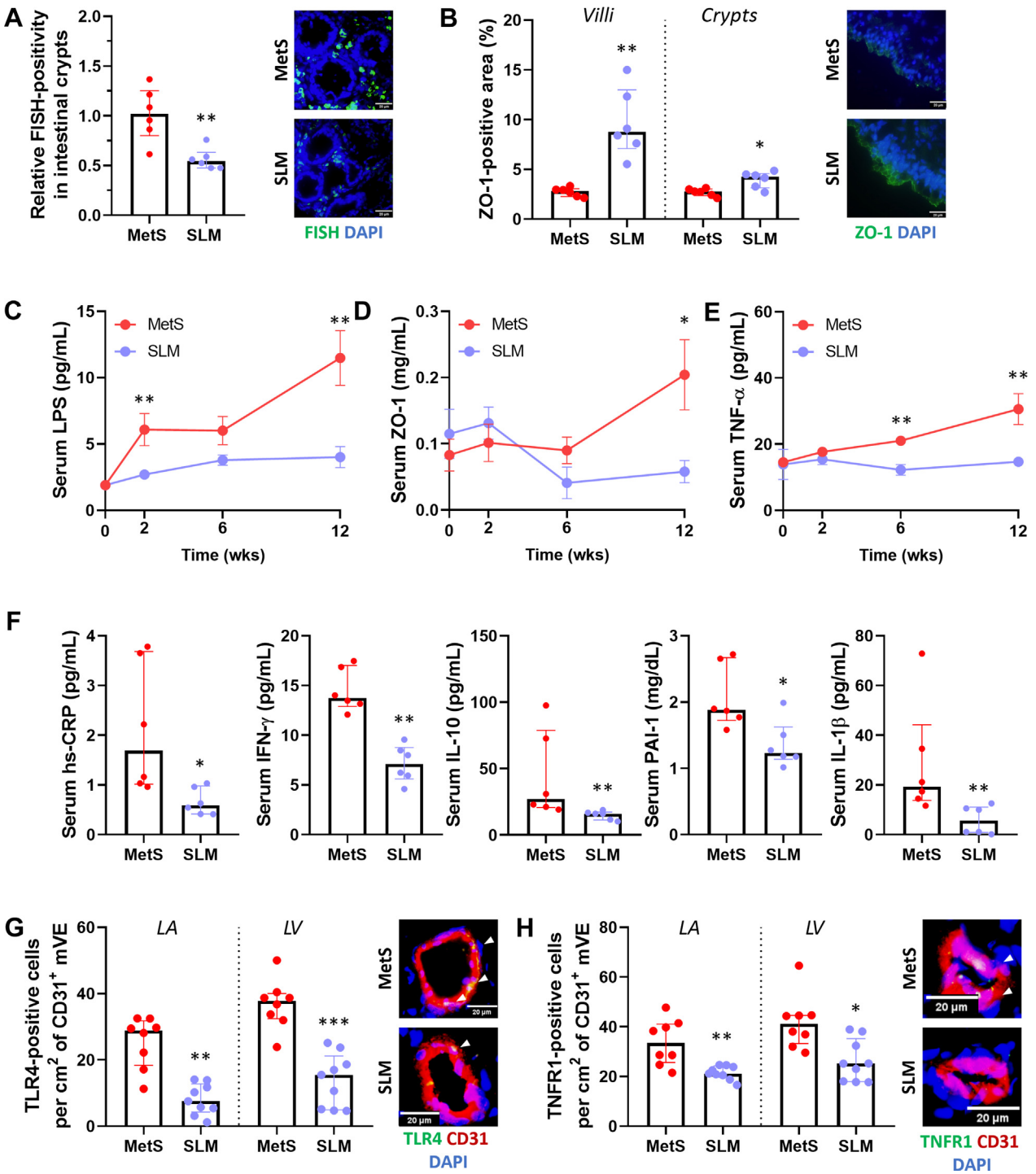


(A) TI FISH labeling of translocating bacteria within crypts and (B) ZO-1 labeling in crypts and villi (MetS: n = 6; SLM: n = 6). (C to F) Time course serum levels of (C) LPS, (D) ZO-1, and (E) TNF-α (at 0, 2, 6, and 12 weeks) and (F) week 12 levels of hs-CRP, IFN-γ, IL-10, PAI-1, and IL-1β (MetS: n = 6; SLM: n = 6). (G, H) LA and LV immunofluorescence labeling of (G) TLR4 and (H) TNFR1 in LA and LV within $CD31^{+}$ mVE (designated by arrowheads) (MetS: n = 8; SLM: n = 9). Representative images were cropped from 600× magnification. Data are presented as median (Q1-Q3) and were compared using the Mann-Whitney test. *$P < 0.05$, **$P < 0.01$, and ***$P < 0.001$. hs-CRP = high-sensitivity C-reactive protein; IFN-γ = interferon gamma; IL = interleukin; LPS = lipopolysaccharide; other abbreviations as in Figures 1 to 3.

**FIGURE 5 Synbiotic Targeting of the Gut-Heart Axis Reduced LA Inflammatory Cell Activity, NLRP3 Signaling, and CM Apoptosis and Decreased TNFR1 and TLR4 Activation in MetS**

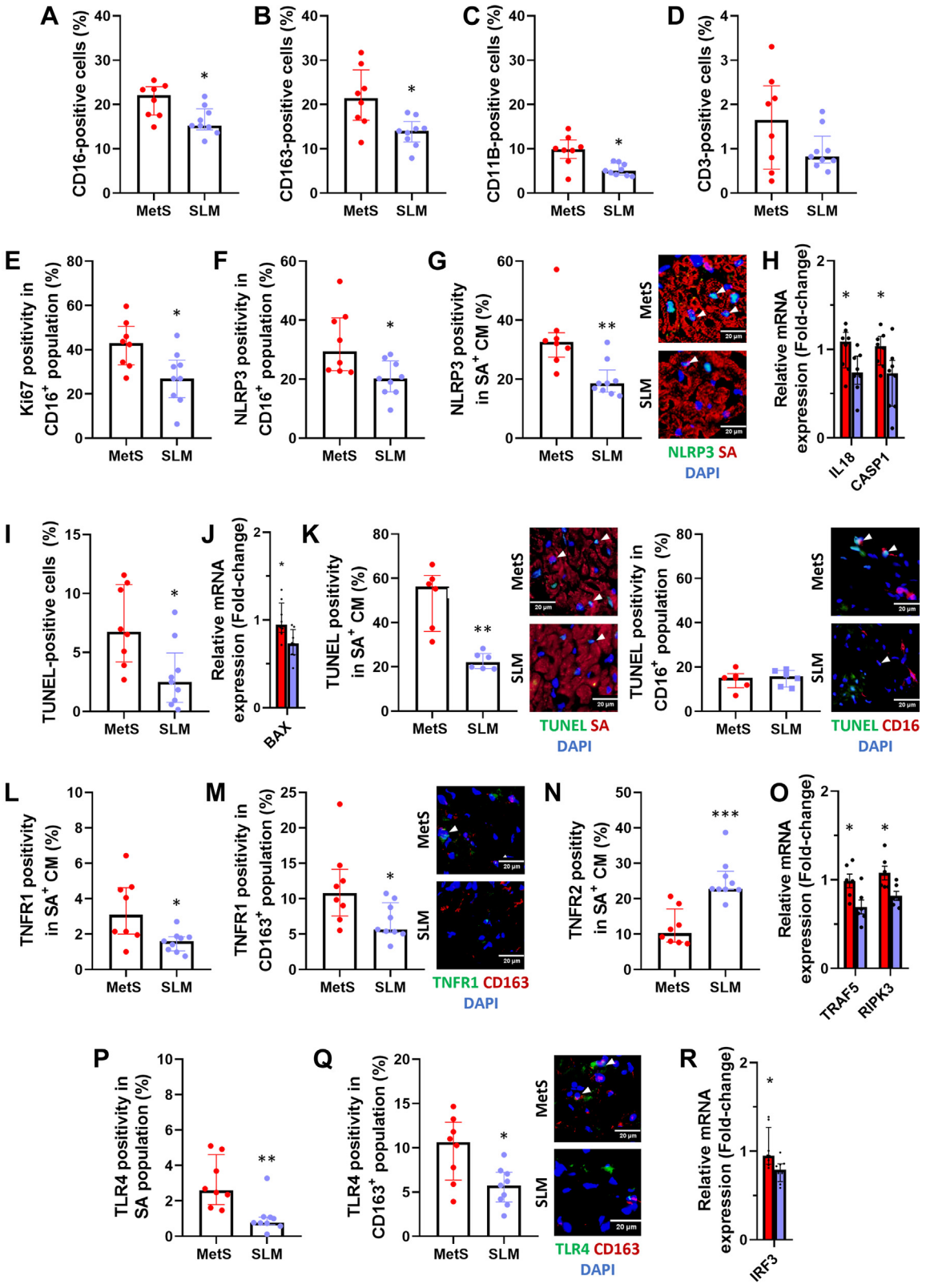


*Continued on the next page*

tissue.[7] The purpose of the current study was: 1) to determine the full temporospatial extent of the GHA in this disease; and 2) to mechanistically determine whether intervention targeted specifically at the gut epithelial level could attenuate inflammation and cardiac structural change in this axis.

Using a human-scale large animal MetS model, we previously showed that derangements in the gut microbiome are associated with progressive development of HFpEF.[8] In the current study, we used the previous MetS animals that demonstrated increased gut dysbiosis as early as 2 weeks after HFSD and identified key temporospatial alignment of gut barrier function loss and evidence of systemic endotoxemia and inflammation beginning at 2 weeks into the study. Our data are consistent with a sequence of events that involve loss of bacterial diversity,[8] increase in gut-resident proinflammatory Gram-negative bacteria associated with mucus layer loss, increased epithelial cell activation and permeability, translocation of bacteria (fluorescence in situ hybridization) and bacterial products (LPS) with activation of inflammatory cells within the gut submucosa and spread of low-grade inflammation to the systemic circulation.

Importantly, we identified a $CD16^+$ cell population within the TI and also within the left heart (LA and LV) that was more activated in MetS and colocalized to proapoptotic and hypertrophic CMs. It is conceivable that these $CD16^+$ cells through paracrine interactions augment CM structural changes within the MetS heart. We identified 2 key cytokine/receptor pathways that can facilitate such cross-talk between Mφs and CMs—namely, TNFR and TLR4—that are known to promote cardiac apoptosis and hypertrophy.[18,20] Support for amplification of these pathways in the gut and heart was evidenced by increased NLRP3 inflammasome expression in epithelial and $CD16^+$ cells within the gut and in CMs and $CD16^+$ cells within the heart, further promoting CM pathologic changes.[21]

A key aspect of this study was the SLM intervention to test whether local targeting of the gut epithelium was sufficient to attenuate inflammation along the GHA. The effects of SLM on cardiac structure were robust and comparable to the effects seen with early use of angiotensin-converting enzyme inhibitors used in rodent models of LVH in the 1980s.[22] Given that LM has previously been shown to reside deep in the mucus layer,[23] it was not surprising that SLM exhibited beneficial effects on epithelial mucus production as well as reducing epithelial cell activation, proliferation, and tight junction protein loss. This effectively "shut down" the gut barrier function loss observed in MetS-alone animals and may have been the key mechanistic benefit of SLM within the TI reducing translocation of whole bacterial populations, bacterial fragments, and LPS, with consequences for reduced gut, circulatory, and cardiac inflammation. Similarly, this benefit extended to the mVE, a key entry point to the heart for systemic inflammatory cytokines, because SLM markedly reduced cognate receptor expression for TNFR1 and TLR4, reducing crossover of this inflammatory cascade from the circulation to the myocardium. Accordingly, CM- and cardiac Mφ-related cytokine receptor pathways of TNFR1 and TLR4 were also markedly attenuated in both the LA and LV by SLM treatment. TNFα inhibitors have previously been shown to contribute to worsening of heart failure in human subjects, presumed due to differential off-target effects on TNFR1 (beneficial) and TNFR2 (deleterious) receptors in the heart.[24] In the current study, SLM treatment decreased TNFR1 and increased TNFR2 expression on CMs in the heart of MetS animals, likely abrogating the perceived dual TNF receptor inhibition effects of existing systemic TNFα inhibitors. Therefore, SLM as a TI-targeted therapy, may circumvent some of the deleterious bireceptor TNF modulatory effects of established pharmacologic inhibitors of TNF-α.[25]

**FIGURE 5 Continued**

(A to E) Immunofluorescence labeling of (A) CD16, (B) CD163, (C) CD11B, and (D) CD3 as a percentage of total LA cells and (E) Ki67 labeling of $CD16^+$ Mφs (MetS: n = 8; SLM: n = 9). (F to H) LA NLRP3 immunofluorescence labeling among (F) $CD16^+$ Mφs and (G) $SA^+$ CMs (designated by arrowheads) (MetS: n = 8; SLM: n = 9) and (H) relative mRNA expression of NLRP3-associated genes (MetS: n = 8; SLM: n = 8). (I) LA TUNEL positivity in total LA cells (MetS: n = 8; SLM: n = 9), (J) relative mRNA expression of proapoptotic gene *BAX* (MetS: n = 8; SLM: n = 8), and (K) TUNEL positivity within $SA^+$ (designated by arrowheads) (MetS: n = 6; SLM: n = 6) and $CD16^+$ cell populations (designated by arrow heads) (MetS: n = 6; SLM: n = 6). (L-O) LA TNFR1 immunofluorescence positivity among (L) $SA^+$ CMs and (M) $CD163^+$ Mφs (designated by arrowheads), (N) TNFR2 positivity among $SA^+$ CMs (MetS: n = 8; SLM: n = 9), and (O) relative mRNA expression of TNFR1-associated genes (MetS: n = 8; SLM: n = 8). (P-R) LA TLR4 immunofluorescence positivity among (P) $SA^+$ CMs and (Q) $CD163^+$ Mφs (designated by arrowheads) (MetS: n = 8; SLM: n = 9) and (R) relative mRNA expression of TLR4-associated gene *IRF3* (MetS: n = 8; SLM: n = 8). All representative images were cropped from 600× magnification. Data are presented as median (Q1-Q3) and were compared using the Mann-Whitney test. *$P < 0.05$, **$P < 0.01$, and ***$P < 0.001$. Abbreviations as in **Figures 1 to 3**.

SLM contains extracellular cytoprotective compounds, the most potent identified to date being exopolysaccharide, a heteropolysaccharide, which we have previously shown has anti-inflammatory effects in murine models of metabolic stress and cardiovascular disease.[26] In contrast to the potential direct effect of SLM-derived exopolysaccharide on epithelial health in the current study, we found no evidence of the indirect effects of SLM, either on the overall composition of the gut bacterial metabolome or on secondary production of specific short-chain fatty acids, such as butyrate, propionate, succinate, or acetate, previously associated with beneficial effects of health-promoting gut bacteria (Supplemental Figure 8). Moreover, SLM had no effect on selected metabolites known to affect inflammation, including trimethylamine-*N*-oxide, or derivatives of tryptophan metabolism (Supplemental Figure 8). Thus, it is unlikely that SLM is acting through known metabolites to effect beneficial changes in the gut epithelial barrier.

**TRANSLATIONAL SIGNIFICANCE.** The MetS model used here replicates almost all of the dietary, microbiome, gut, circulatory, and heart aspects of human cardiometabolic disease.[27] The clinical scale of the model and the anti-inflammatory effects of the synbiotic intervention used raises the possibility of a new gut-directed therapeutic paradigm targeting LVH and LA myopathy in the context of HFpEF. Although further preclinical studies are warranted, our data indicate a potentially groundbreaking disease-modifying therapy for patients with cardiometabolic disease. Future studies should look at mining compounds both from within and on the surface of bacteria to determine the druggability of this effect.

**STUDY LIMITATIONS.** The pigs used in this study were all female (because of concerns regarding growth, handling, and male aggression), and thus extrapolation to male subjects needs to be done with caution, although the literature supports cardiometabolic disease being more prominent in males compared to females. These animals were also young and in their growth phase and therefore do not represent mature adults. The current Landrace model is well established as a model for HFpEF and MetS but lacks some of the additional nuanced translational elements of Ossabaw and other specialized porcine breeds in terms of obesity and full-blown diabetes—something we recently reviewed in detail.[28] The current porcine study is limited to 12 weeks, whereas cardiometabolic disease in human subjects develops over decades, and the sample sizes used were modest although statistically significant. Similarly, this time limitation extends to the duration of treatment with the synbiotic, which may be different in human disease, where longer-term intervention may be required. Moreover, the current intervention model reflects more disease prevention, and it remains to be proven whether such intervention reverses preexisting structural heart changes in MetS established over many years.

## CONCLUSIONS

Our study suggests a poor diet-microbiome interface drives epithelial barrier dysfunction, augmenting gut, blood, and cardiac inflammatory aspects of the GHA. The proposed gut-directed synbiotic targeting of this axis has the potential to reduce the structural heart changes in the LA and LV induced by MetS, which may be complementary to current risk factor reduction approaches in this disease. These data support wider research on the gut epithelial barrier as an important gatekeeper of inflammation in cardiometabolic disease.

**ACKNOWLEDGMENTS** The authors thank Vincent Mehigan, Kerry Carlile, Siddhant Gawli, Elisa Michel, Janet Choi, Dr Huimin Ye, Dr Klara Vlckova, Dr Derek Whelan, Dr Jonathan Breton, and Dr Cara Hueston for protocols/technical support; MS-Omics for assistance in metabolome analysis; and Vincent Mehigan, Kerry Carlile, and Siddhant Gawli for support with animal husbandry and care. The authors acknowledge as well the Teagasc Moorepark sequencing team.

## FUNDING SUPPORT AND AUTHOR DISCLOSURES

This study was funded by a grant from Tate and Lyle Solutions USA LLC and by a grant from Science Foundation Ireland to the Alimentary Pharmabiotic Centre at University College Cork, grant number 12/RC/2273-P2. Drs Herisson, Karnik, Laurie, Canene-Adams, Ross, Stanton, Caplice are named inventors on intellectual property co-owned by University College Cork and Tate and Lyle Solutions, LLC relating to synbiotic treatment of metabolic syndrome. All other authors have reported that they have no relationships relevant to the contents of this paper to disclose.

**ADDRESS FOR CORRESPONDENCE:** Dr Noel Caplice, PI Alimentary Pharmabiotic Centre, Room 2.40, Bioscience Institute, University College Cork, College Road, Cork, Ireland. E-mail: n.caplice@ucc.ie.

## PERSPECTIVES

**COMPETENCY IN MEDICAL KNOWLEDGE:** In a porcine model of diet-induced cardiometabolic disease, a synbiotic (*Lactobacillus mucosae* + fiber) reduces LA myopathy and LVH through attenuation of the gut-heart inflammatory axis. Targeting this axis may offer new avenues for the treatment of cardiometabolic disease.

**TRANSLATIONAL OUTLOOK:** Further research is required to translate these experimental findings to clinical application of either synbiotics or bacterial-derived products as a potential therapeutic approach to patients with metabolic syndrome, LA myopathy, and LVH.

## REFERENCES

**1.** Lusis AJ, Attie AD, Reue K. Metabolic syndrome: from epidemiology to systems biology. *Nat Rev Genet*. 2008 Nov;9(11):819–830.

**2.** Borlaug BA, Sharma K, Shah SJ, Ho JE. Heart failure with preserved ejection fraction: *JACC* scientific statement. *J Am Coll Cardiol*. 2023;81:1810–1834.

**3.** Usman MS, Siddiqi TJ, Anker SD, et al. Effect of SGLT2 inhibitors on cardiovascular outcomes across various patient populations. *J Am Coll Cardiol*. 2023;81(25):2377–2387.

**4.** Murphy SP, Kakkar R, McCarthy CP, Januzzi JL. Inflammation in heart failure: *JACC* state-of-the-art review. *J Am Coll Cardiol*. 2020;75(11):1324–1340.

**5.** Di Vincenzo F, Del Gaudio A, Petito V, Lopetuso LR, Scaldaferri F. Gut microbiota, intestinal permeability, and systemic inflammation: a narrative review. *Intern Emerg Med*. 2024;19(2):275–293.

**6.** Matsiras D, Bezati S, Ventoulis I, Verras C, Parissis J, Polyzogopoulou E. Gut failure: a review of the pathophysiology and therapeutic potentials in the gut-heart axis. *J Clin Med*. 2023;12(7):2567.

**7.** Desai D, Desai A, Jamil A, et al. Re-defining the gut heart axis: a systematic review of the literature on the role of gut microbial dysbiosis in patients with heart failure. *Cureus*. 2023;15(2):e34902.

**8.** O'Donovan AN, Herisson FM, Fouhy F, et al. Gut microbiome of a porcine model of metabolic syndrome and HF-pEF. *Am J Physiol Heart Circ Physiol*. 2020;318(3):H590–H603.

**9.** Beale AL, O'Donnell JA, Nakai ME, et al. The gut microbiome of heart failure with preserved ejection fraction. *J Am Heart Assoc*. 2021;10(13):e020654.

**10.** Russell WMS, Burch RL The Principles of Humane Experimental Technique. 1959.

**11.** Xia J. Using MetaboAnalyst 3.0 for comprehensive metabolomics data analysis. *Curr Protoc Bioinformatics*. 2016;15(1):14.10.1–14.10.91.

**12.** Schwarzl M, Hamdani N, Seiler S, et al. A porcine model of hypertensive cardiomyopathy: implications for heart failure with preserved ejection fraction A porcine model of hypertensive cardiomyopathy: implications for heart failure with preserved ejection fraction. *Am J Physiol Heart Circ Physiol*. 2015;309:1407–1418.

**13.** Snarski P, Sukhanov S, Yoshida T, et al. Macrophage-specific IGF-1 overexpression reduces CXCL12 chemokine levels and suppresses atherosclerotic burden in Apoe-deficient mice. *Arterioscler Thromb Vasc Biol*. 2022;42(2):113–126.

**14.** Haanen C, Vermes I. Apoptosis and inflammation. *Mediators Inflamm*. 1995;4(1):5–15.

**15.** Jacoby JJ, Kalinowski A, Liu MG, et al. Cardiomyocyte-restricted knockout of STAT3 results in higher sensitivity to inflammation, cardiac fibrosis, and heart failure with advanced age. *Proc Natl Acad Sci U S A*. 2003;100(22):12929–12934.

**16.** Marín-Aguilar F, Lechuga-Vieco AV, Alcocer-Gómez E, et al. NLRP3 inflammasome suppression improves longevity and prevents cardiac aging in male mice. *Aging Cell*. 2020;19(1):e13050.

**17.** Markowiak P, Ślizewska K. Effects of probiotics, prebiotics, and synbiotics on human health. *Nutrients*. 2017;9. https://doi.org/10.3390/nu9091021

**18.** Katare PB, Nizami HL, Paramesha B, Dinda AK, Banerjee SK. Activation of toll like receptor 4 (TLR4) promotes cardiomyocyte apoptosis through SIRT2 dependent p53 deacetylation. *Sci Rep*. 2020;10(1):19232.

**19.** Haudek SB, Taffet GE, Schneider MD, Mann DL. TNF provokes cardiomyocyte apoptosis and cardiac remodeling through activation of multiple cell death pathways. *J Clin Invest*. 2007;117(9):2692–2701.

**20.** Yokoyama T, Nakano M, Bednarczyk JL, McIntyre BW, Entman M, Mann DL. Tumor necrosis factor-alpha provokes a hypertrophic growth response in adult cardiac myocytes. *Circulation*. 1997;95(5):1247–1252.

**21.** Suetomi T, Willeford A, Brand CS, et al. Inflammation and NLRP3 inflammasome activation initiated in response to pressure overload by $Ca^{2+}$/calmodulin-dependent protein kinase II δ signaling in cardiomyocytes are essential for adverse cardiac remodeling. *Circulation*. 2018;138(22):2530–2544.

**22.** Fernandez D, Bolli P, Snedden W, Vasdev S, Fernandez PG. Modulation of left ventricular hypertrophy by dietary salt and inhibition of angiotensin converting enzyme. *J Hypertens Suppl*. 1988;6(4):S145–S147.

**23.** Van den Abbeele P, Roos S, Eeckhaut V, et al. Incorporating a mucosal environment in a dynamic gut model results in a more representative colonization by lactobacilli. *Microb Biotechnol*. 2012;5(1):106–115.

**24.** Chung ES, Packer M, Lo KH, Fasanmade AA, Willerson JT. Randomized, double-blind, placebo-controlled, pilot trial of infliximab, a chimeric monoclonal antibody to tumor necrosis factor-α, in patients with moderate-to-severe heart failure: results of the Anti-TNF Therapy Against Congestive Heart Failure (ATTACH) trial. *Circulation*. 2003;107(25):3133–3140.

**25.** Rolski F, Błyszczuk P. Complexity of TNF-α signaling in heart disease. *J Clin Med*. 2020;9:1–24.

**26.** Ryan PM, Stolte EH, London LEE, Wells JM, Long SL, Joyce SA, et al. *Lactobacillus mucosae* DPC 6426 as a bile-modifying and immunomodulatory microbe. *BMC Microbiol*. 2019;19(1):1–13.

**27.** Mechanick JI, Farkouh ME, Newman JD, Garvey WT. Cardiometabolic-based chronic disease, addressing knowledge and clinical practice gaps. *J Am Coll Cardiol*. 2020;75(5):539–555.

**28.** Cluzel GL, Ryan PM, Herisson FM, Caplice NM. High-fidelity porcine models of metabolic syndrome: a contemporary synthesis. *Am J Physiol Endocrinol Metab*. 2022;322(4):E366–E381.

**KEY WORDS** heart failure, metabolic syndrome, microbiome, synbiotic

**APPENDIX** For an expanded Methods section and supplemental tables and figures, please see the online version of this paper.